ChemPubSoc Europe

DOI: 10.1002/syst.201900011

CHEMSYSTEMSCHEM Articles

VIP *Very Important Paper*

Special Collection

Chemobrionic Fabrication of Hierarchical Self-Assembling Nanostructures of Copper Oxide and Hydroxide

Elizabeth Escamilla-Roa,[a, b] Julyan H. E. Cartwright,*[b, c] and C. Ignacio Sainz-Díaz[b]

Copper oxide nanostructures have great potential use in a plethora of nanotechnology applications including nanoelectronics, photovoltaics, sensors, electrochemistry, and pharmacology. In the present work we show how hierarchically nanostructured copper oxide and hydroxide may be prepared through self-assembly from $CuSO_4$ salt and silicate solutions using the chemobrionic growth process of a chemical garden. Procedures were explored using the cupric salt in either solid (pellet and seed growth methods) or liquid phase (fluid injection techniques). Self-assembling nanostructures were characterized by means of environmental scanning electron microscopy (ESEM) with energy-dispersive X-ray spectroscopy (EDX) analysis, micro-Raman spectroscopy and X-ray diffraction. Our results show the formation of crystalline aggregates of copper oxide and hydroxide in complex hierarchical nanostructured forms including fans, flowers, petals, skeins, lentils, and sheaves. Analytical methods corroborate that these nanostructures may be selected in shape and chemical composition with the reaction conditions.

1. Introduction

Copper oxide nanostructures are becoming of increasing technological importance.[1–6] Among a plethora of applications, nanoparticles and nanostructures formed of metal oxides such as CuO are of particular interest in nanotechnology as superconductors,[7] as supercapacitors,[8] as sensors[9] and as battery anodes,[10] in materials science as catalysts[11,12] and as materials with enhanced photocatalytic properties[13,14] and in pharmacology as antibacterial materials.[15,16] Likewise, copper hydroxide nanoparticles have found applications for their antimicrobial[17] and for their antitoxicity properties.[18] While there exist many routes to the fabrication of such nanostructures, new and, in particular, simple and selectable routes involving self-assembly rather than many complicated steps are clearly of much interest.

Chemical gardens are biomimetic plant-like structures formed abiotically by metallic salts when immersed in a solution with specific anions.[19] A semipermeable membrane is formed surrounding the salt seed impeding the outflow of ions from the seed while allowing the inflow of water from the external solution driven by osmosis. The membrane swells as more water dissolves the salt seed. This water inflow into the membrane increases the internal pressure. Depending on the properties of the membrane, this can increase its volume or break it. In the latter case, the internal solution flows out reacting with the external solution forming a tube around the flow growing by precipitation. The morphology of the structures formed is a product of forced convection, driven by osmotic pressure, owing to the semipermeable membrane, and free convection from buoyancy, since the ejected solution generally has a different density than the external solution. The final result is a combination of three-dimensional structures of different sizes and shapes, resembling a garden with plants.[20] The new field developing from these concepts is termed chemobrionics.[19] Previous works have studied structures of copper (II) sulfate formed from silicate chemical gardens for various concentrations of silicate, and have determined the tubular growth and composition with various analytical methods.[21–27] It should also be noted that microtube formation related to chemical-garden formation is observed in iron corrosion,[19] while copper hydroxides-sulfates have great environmental interest and are often found in the corrosion of bronze structures.[28]

In this study we explore with this technique new routes to the formation of a great variety of self-assembling nanostructures from reactions of $CuSO_4$ with silicate in alkaline conditions, obtaining CuO and $Cu(OH)_2$ crystals and $Cu_x(SO_4)_y \cdot Cu(OH)_z$ complexes. Nanostructures have been obtained in two phases: solid-liquid (pellets and seed growth method) and liquid-liquid (injection of dissolved salt). Structures were characterized by means of environmental scanning electron microscopy (ESEM) with energy-dispersive X-ray spectroscopy (EDX) analysis, micro-Raman spectroscopy and X-ray diffraction. The forms obtained, such as flowers, lentils, fans, wheat sheaves and petals, are reminiscent of biological morphologies. The morphology and composition may be selected according to the growth method and reaction conditions.

[a] *E. Escamilla-Roa*
Department of Computer Science, Electrical and Space Engineering, Luleå University of Technology, 97187 Luleå, Sweden
[b] *E. Escamilla-Roa, J. H. E. Cartwright, C. I. Sainz-Díaz*
Instituto Andaluz de Ciencias de la Tierra, CSIC-Universidad de Granada, E-18100 Armilla, Granada, Spain
E-mail: julyan.cartwright@csic.es
[c] *J. H. E. Cartwright*
Instituto Carlos I de Física Teórica y Computacional, Universidad de Granada, E-18071 Granada, Spain

Special Collection *An invited contribution to a Special Collection on Systems Chemistry Applied to Materials Science*

© 2019 Wiley-VCH Verlag GmbH & Co. KGaA, Weinheim

2. Results and Discussion

2.1. Self-Assembly by Solid-Liquid Phase Techniques

Two concentrations of sodium silicate solution were used: 0.1 M and 1 M. With 1 M sodium silicate, numerous self-assembling tubular structures were obtained with a copper sulfate seed (Figure 1a). However, with 0.1 M sodium silicate, only a large bubble structure was formed and no tube formation was observed (Figure 1b). In the pellet method the precipitation process with 1 M sodium silicate formed numerous, large and fine tubes of intense blue colour of approximately 20 cm length having an overall appearance similar to tree branches (Figure 1c, d).

ESEM micrographs of these samples displayed the micromorphology of the tubular structures (Figure 2). The samples obtained with a seed show smooth and porous external surfaces and heterogeneous internal surfaces with many small crystals (Figure 2a). These crystals were observed also on the tips of the tubes (Figure 2b). Several morphologies are observed in a disordered heterogeneous distribution: round and oval nanopellets, needles, and crystal aggregates resembling sheaves (Figure 2c). The tubular structures obtained from pellet-growth experiments show different and peculiar crystal structures in the inner surface of tubes, such as lentils (Figure 2d,e), flowers (Figure 2f–j) and hierarchical crosslinked discs (Figure 2k). The micrographs show that crystals forming the lenticular morphology are compact and can be separated from the tube. They are ellipsoidal discs of 2–5 μm average diameter and some 200 nm in thickness. Some of these discs form aggregates in which helical growth patterns from screw dislocations can be observed (Figure 2e). Structures with a flower-like morphology also grew in the inner surface of tubes. These microstructures that resemble flowers are composed of crystals in densely packed nanorods. Some of them develop petals of an irregular rectangular shape with a size of approximately 30 μm, with numbers of them terminating in peaks. After grinding partially these flowers, their nanostructure is observed. These petal-like structures have a smooth surface with a thickness of 3–4 μm and are composed of an aggregate of many needle crystals oriented parallel along the surface with an average diameter of 100–200 nm, growing towards the apex of the petal. Moreover, another order of nanostructure can be observed in the sides of these petals, indicating that the above needles are <1 μm long, being a superposition of many crystals (Figure 2i,j). It may be noted that a similar self-organization is observed to be formed by biomineralization in the crossed-lamellar structures of mollusc shells.[29] Further hierarchical self-organization was observed in the internal surface of tubes where units of ellipsoidal morphology with an average dimension of 4×2 μm by 200 nm are stacked forming parallel sheets (Figure 2k). This morphology resembles the nanostructure observed in butterfly wings (Figure 2l).[30]

The chemical composition of the structures in the inner surface of self-assembling tubes was determined in situ by EDX analysis of the sample within the ESEM. The structures formed in the inner surface of the tubes grown from copper sulphate seed showed a much larger elemental proportion of Cu and O than Si and S, indicating the presence of copper oxide/hydroxides (Figure 3a–c), in accord with previous studies.[22] All structural morphologies showed similar chemical composition. The external surface has a high content of Si. Some crystals with rectangular tabular morphology are found with a high content of S, O, and Cu that can be assigned to copper sulfate (Figure 3d). Small crystals are formed on the external surface with a high content of Cu and O and a certain amount of S, indicating in this case the presence of copper oxide/hydroxide along with copper sulphate (Figure 3c,d,e).

To corroborate a gradient of chemical composition in which the interior surface is rich in copper and the exterior surface is rich in silicon, we performed a micro-Raman analysis of tubes obtained from pellet growth (Figure 3f). Two bands characteristic of $Cu(OH)_2$ appear at around 397 and 479 cm^{-1}, which might however correspond also to the copper hydroxide-sulfate, langite, $Cu_4(SO_4)(OH)_6 \cdot 2H_2O$, bands at 391 and 481 cm^{-1}.[28] The presence of silicate can be observed with the

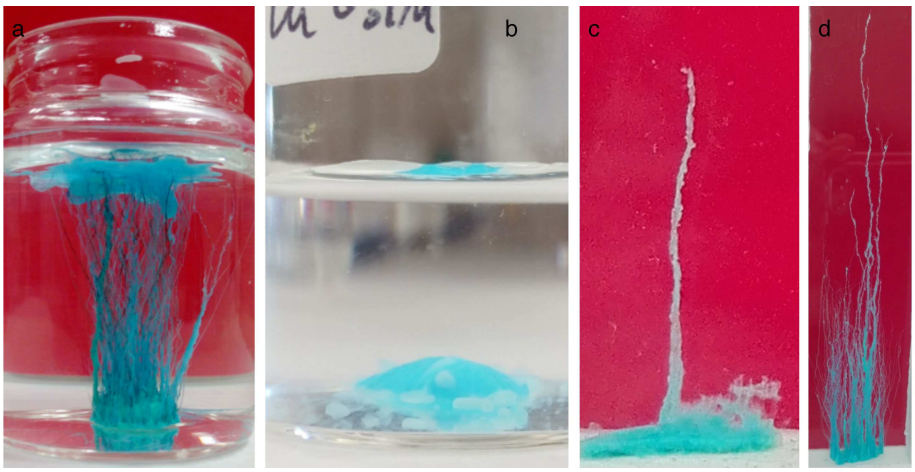

Figure 1. Tubular structures obtained by solid-liquid phase techniques. (a,b) A $CuSO_4$ seed in sodium silicate solutions of (a) 1 M and (b) 0.1 M, and (c,d) a $CuSO_4$ pellet in 1 M sodium silicate solution.

© 2019 Wiley-VCH Verlag GmbH & Co. KGaA, Weinheim

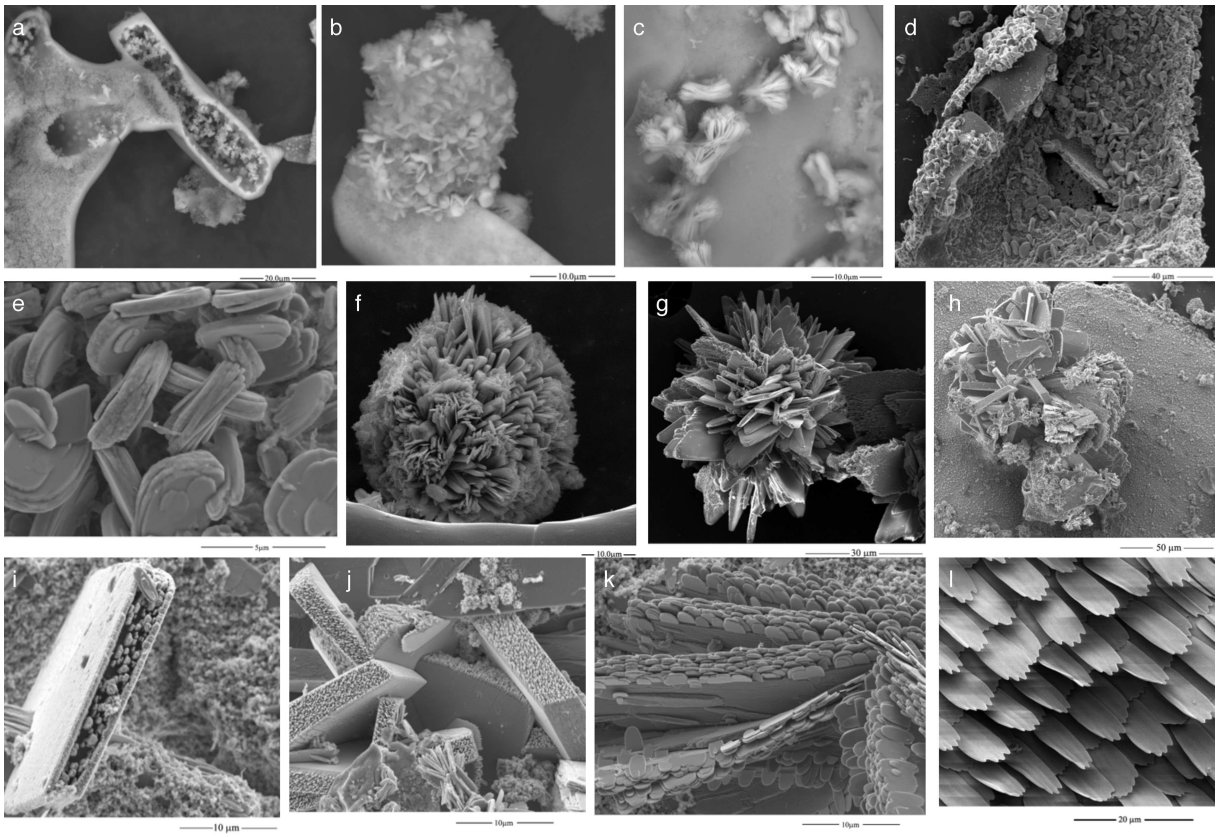

Figure 2. Nanostructures obtained by solid-liquid phase techniques. ESEM micrographs of (a,b,c) the inner surface of a tube grown using a seed of $CuSO_4$ in 1 M sodium silicate solution; (d,e) tubes grown from pellets; (f–j) structures with the appearance of flowers and petals on the inner surface of tubes grown from pellets; (k) structures with butterfly-wing-like morphology observed inside the tubes grown from pellets; compare with (l) an actual butterfly wing.

stretching Si–O bands at 974 cm^{-1}, however, this band can correspond also to the sulfate stretching band of copper hydroxide-sulfates. Menor-Salvan et al.[31] assigned this band to brochantite, $Cu_4(SO_4)(OH)_6$, whereas Martens et al.[28] assigned it to langite. In addition, other characteristic peaks of CuO at 256, 321 and 610 cm^{-1} are observed, according with previous studies on copper oxides where Raman spectra of CuO were reported with characteristic peaks at 250, 300, 347 and 635 cm^{-1}.[32,33] Nevertheless, the broad band at 610 cm^{-1} can be assigned also to brochantite. This is confirmed with the bands overlapped in the broad band at 1050–1150 cm^{-1} range.[28]

2.2. Self-Assembly by Liquid-Liquid Phase Techniques

Two techniques were used, direct and reverse injection,[34] in which the hydrated salt, $CuSO_4$, was injected in dissolved form. In the first case aqueous solutions of the salt of 0.05–0.5 M concentration were injected into a reactor containing 15–30 mL of 1 M silicate solution at a constant rate of 3 mL/h (Figure 4). The total volume of salt injected was 1 ml. With 0.05 M copper sulphate, the formation of tubes was slow with several side tubes surrounding the main tube of a light blue colour (Figure 4a). The precipitation process using 0.5 M copper sulphate formed a large tubular structure of approximately 25 cm length and of an intense blue colour (Figure 4b). In the upper part of the tube, the walls are at first partially transparent light blue and become more irregular towards a transparent tip (Figure 4c). After some hours the whole tube became an intense blue colour. In the second technique of reverse injection, 1 mL of silicate solutions of 0.1 or 1 M concentration were injected at a constant rate of 3 mL/h into 15 mL of 0.25 M copper salt solution of pH ~ 2.6. With 1 M silicate, blue tubular structures of approximately 5 cm length were formed. With 0.1 M sodium silicate, the tubular structures were more heterogeneous and an amount of silicate did not precipitate along the tubes but at the top of the solution (Figure 4d). Only the tubular structures formed from the higher, 1 M, silicate concentration were stable, whereas the structures formed with 0.1 M silicate redissolved after some hours. In general this method produced a principal tube seen under an optical microscope to have a rough and heterogeneous surface with multiple interconnected channels (Figure 4e,f).

ESEM micrographs of the structures formed showed a smooth external surface and flower-like microstructures recalling chrysanthemum flowers (Figure 5a–e) in the inner surface of the tubes. These flowers are similar to those observed with the pellet-growth method (Figure 2f,g) but with sharper, pointed terminations. Besides, microstructures formed with sole-shaped crystals were also found in these structures (Figure 5i–k). These

© 2019 Wiley-VCH Verlag GmbH & Co. KGaA, Weinheim

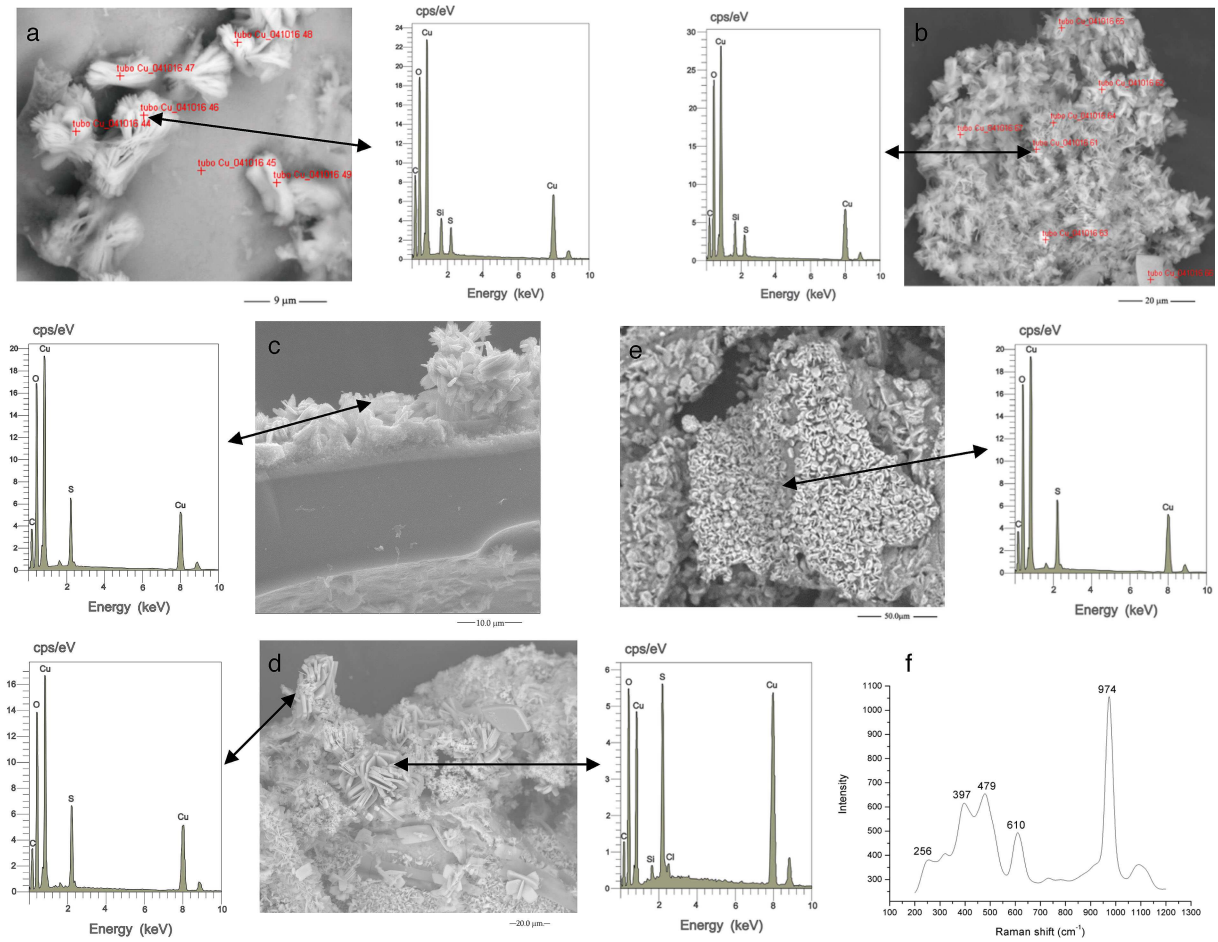

Figure 3. Chemical microanalyses of materials obtained by solid-liquid phase techniques. (a,b) Internal surface of tubular structures from seed; (c,d,e) internal surface of tubular structures formed from pellet; (f) micro-Raman spectrum corresponding to tubes formed from pellet.

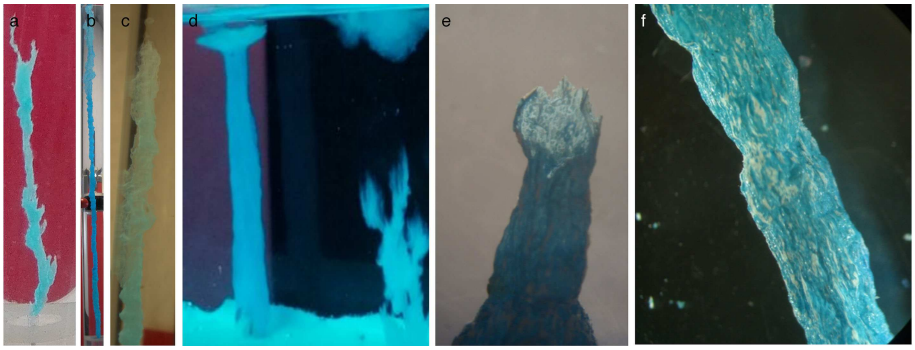

Figure 4. Tubular structures obtained by liquid-liquid phase techniques. (a) Injection of 0.05 M $CuSO_4$, and (b,c) 0.5 M $CuSO_4$ into 1 M silicate solution, and (d) reverse injection of (right structure) 0.1 M silicate solution and (left structure) 1 M silicate solution into 0.25 M $CuSO_4$ solution. (e,f) Aspect of tubular structures obtained from 0.5 M $CuSO_4$ injection into silicate solution observed with an optical microscope.

are similar to those obtained from pellet growth (Figure 2k), however the 3D disposition of these microstructures is more disordered and different to that found in the procedure starting from a pellet. Further biomimetic forms found with this growth method (Figure 5g–k) include fans and wheat sheaves, formed by intercrossed sheaves of needles of 10 μm length and 500–1000 nm diameter. From this perspective, the tube has a section wherein the crystalline flowers grow and another part shows a porous wall without flowers. Other biomimetic crystalline forms are observed at small sizes between 5 and 20 μm.

Chemical analysis (Figure 6a–c) indicates that in the injection method, structures are formed by Cu and O. The content of

© 2019 Wiley-VCH Verlag GmbH & Co. KGaA, Weinheim

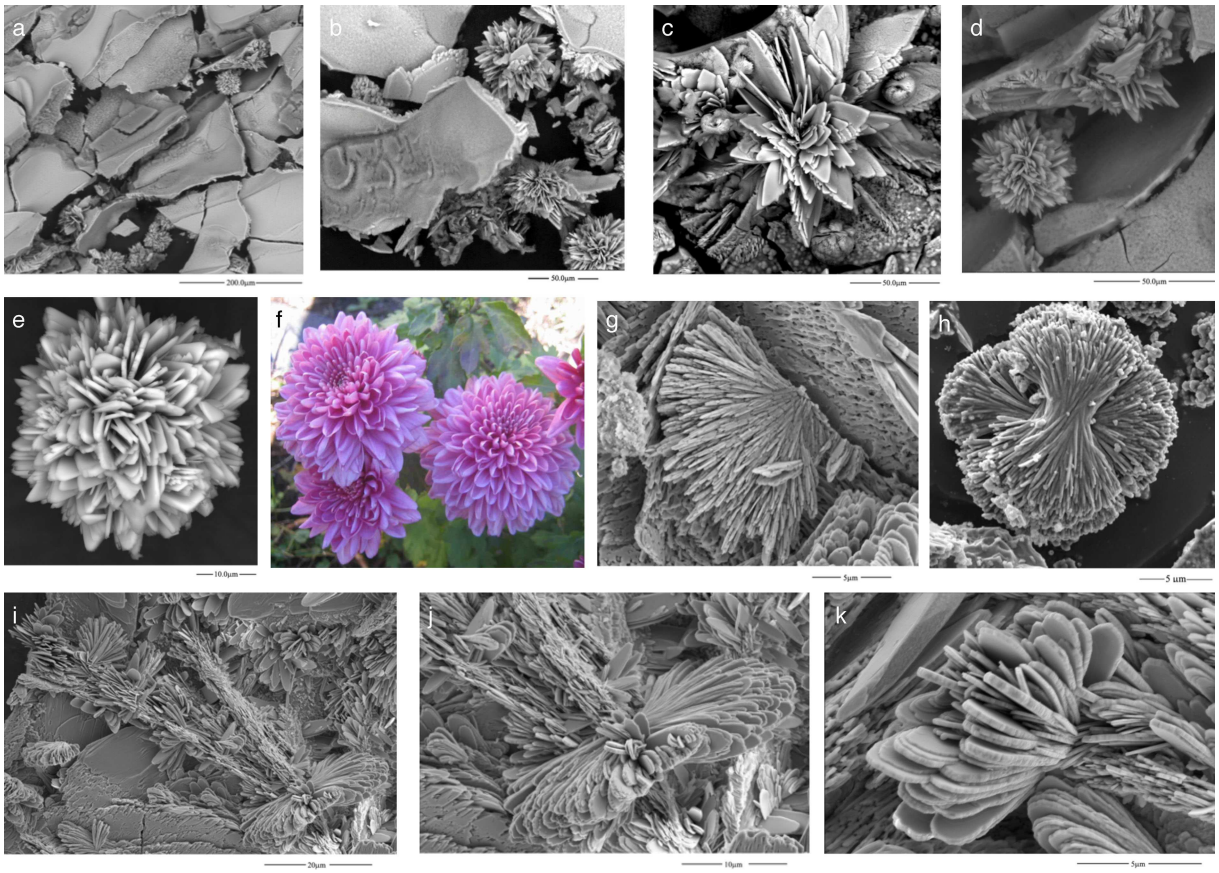

Figure 5. Nanostructures obtained by liquid-liquid phase techniques. ESEM micrographs of structures produced by injection of $CuSO_4$ into silicate solution. (a–e) Flower-like nanostructures may be compared to (f) actual chrysanthemum flowers; (g–k) other nanostructures are fans, sheaves of wheat and soles.

these elements is larger than the Si and S content. This analysis indicates that the composition of these crystalline forms is mainly copper oxide/hydroxide with the presence of a hydrated copper sulphate or mixed copper sulphate/oxide/hydroxide structures. On the other hand, in the external surface Si is a major element, indicating that this surface is formed mainly by silicates. Micro-Raman analysis (Figure 6d) shows several peaks in the spectrum that are characteristic of CuO at 248, 320 and 615 cm^{-1}. The $Cu(OH)_2$ peaks appear at 392 and 480 cm^{-1}. A band that appears at around 973 cm^{-1} may be assigned to the stretching motions in the Si–O–Si bonds, but also it can be assigned to the stretching mode of hydrated copper sulfate-oxide-hydroxides, as noted above. The bands at 590–630 cm^{-1} and 1050–1150 cm^{-1} can be assigned also to brochantite.[28]

Lastly, we present results obtained with reverse injection, in which the external copper sulfate medium of precipitation had a low pH and the basic silicate solution was injected. As before, micrographs of the samples were acquired by ESEM (Figure 7). Nanostructures with several morphologies can be distinguished. One such nanostructure is discs of 2 μm diameter and a thickness of 200–400 nm that form microstructures with an appearance of complex skeins (Figure 7a–c). At the same time, an additional nanostructure can be observed: these discs are formed by quasi-spherical nanoparticles of about 1 nm^3 in average size. These nanoparticles can be considered the aggregation units that form the whole microstructure (Figure 7c). A further development of these microstructures can be observed in which there is growth in one direction, perpendicular to the nucleation plane, generating a further morphology (Figure 7d). Another morphology observed is of linear nanoneedles of some 500 nm width and 10 μm length that stack parallel forming flake microstructures of 2 μm width. In some cases these nanoneedles form monolayer flakes and in others, multilayer bunches (Figure 7e,f). These microstructures are randomly distributed on the internal surface of tubes, however at an initial stage it seems that they begin growing from the membrane in a perpendicular direction (Figure 7g). Other microstructures having flower-like morphologies are observed growing on the internal surface of tubes (Figure 7h–n). In some cases these microstructures participate in the tip closure of microtubes (Figure 7h). These flower-like microstructures are 20–40 μm in diameter (Figure 7k–n) and similar to those previously described. The components of these microstructures can be seen to be petal-like forms of 300–1000 nm in thickness terminating in square or pyramidal tips. An intermediate growth stage of these microstructures is noted in which their ultrastructure is observed. The petal-like forms are formed by stacking of needles that grow in a perpendicular direction from

© 2019 Wiley-VCH Verlag GmbH & Co. KGaA, Weinheim

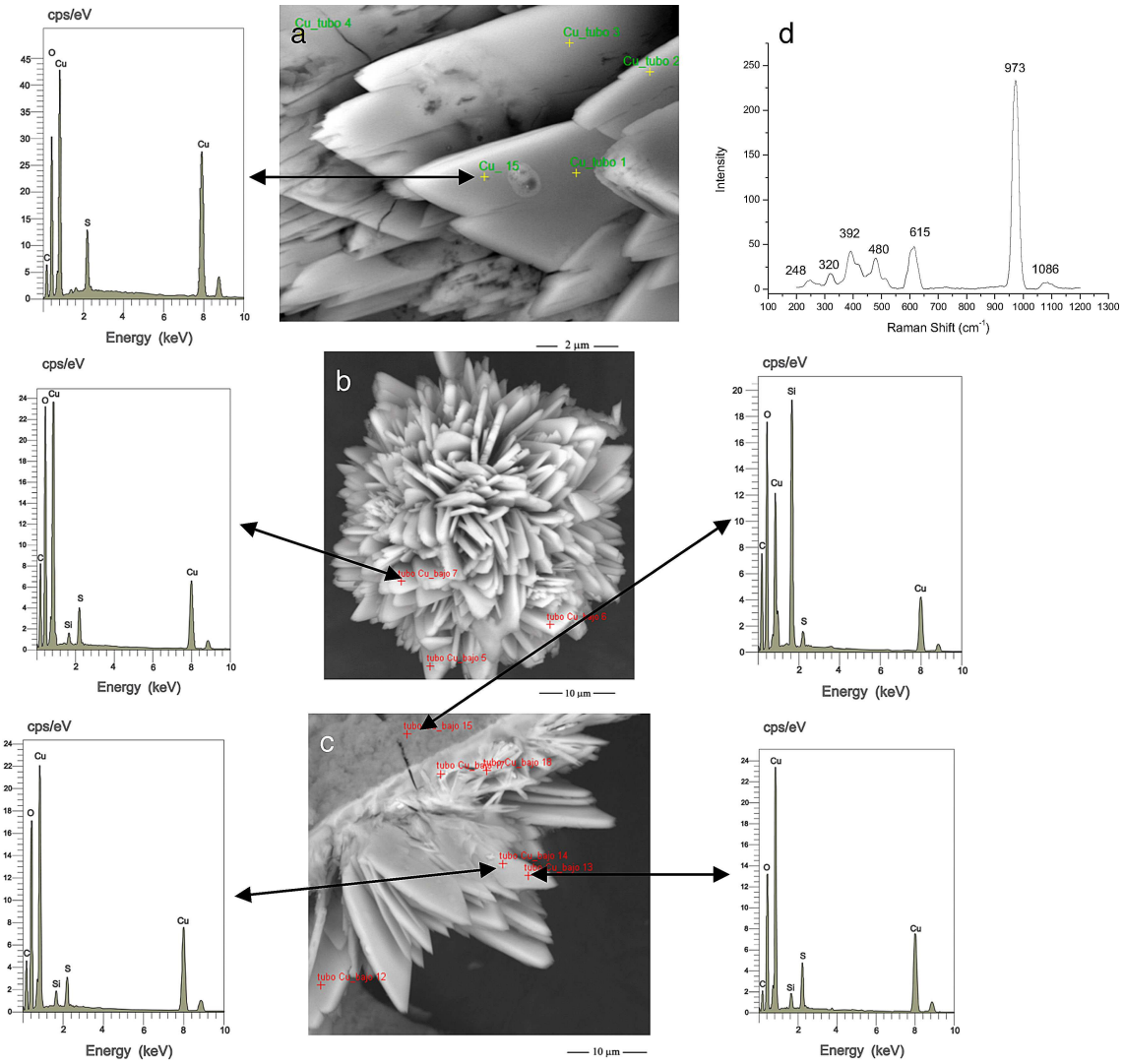

Figure 6. Chemical microanalyses of materials obtained by liquid-liquid phase techniques. (a–c) Internal surface of tubular structures formed from injection of $CuSO_4$ into silicate solution; (d) micro-Raman spectrum corresponding to tubes obtained by the injection method

the microstructure base. The tips of the needles are growing faster than the whole petal (Figure 7k). Possibly, after the stacking of needles lateral crystal growth is produced forming a uniform surface of the petal. This ultrastructure is similar to that detected above in experiments with pellet growth (Figure 2j) but here the needles are thicker.

The chemical analysis of the morphology observed by ESEM was performed in situ using EDX analysis (Figure 8). The flower-like microstructures are formed mainly of Cu and O with small proportion of S and Si. The content of Si increases drastically in the external surface. In some flowers, the content of S is higher but the predominance is of Cu and O. Hence, these microstructures are formed by copper oxide/hydroxides with impurities of copper sulfate or copper complexes of sulphate/hydroxide with several hydration levels.

2.3. X-Ray Diffraction Results

Precipitates were milled to powder and the resulting powder X-ray diffraction patterns showed some differences between the solids obtained from seeds and pellets and those obtained from the injection methods (Figure 9). No crystallographic differences were observed between the lower and tip zones of tubular structures formed from pellets. The proportion of amorphous or not very crystalline phases is higher in the solids obtained by the injection technique, as was expected since this growth process is much faster than that from a seed pellet. The main crystalline structures detected in the powder X-ray diffraction profile of the solids obtained from pellets are also detected in the solids obtained from injection. No reflections of copper sulfate pentahydrate crystals are observed.[6] In both sets of results a small amount of halite can be noted, assigning to it the reflections at 28°, 31°, and 45.5° (2θ units). The reflections at 14°, 23°, 27°, and 36° (2θ units) observed in both results can be

© 2019 Wiley-VCH Verlag GmbH & Co. KGaA, Weinheim

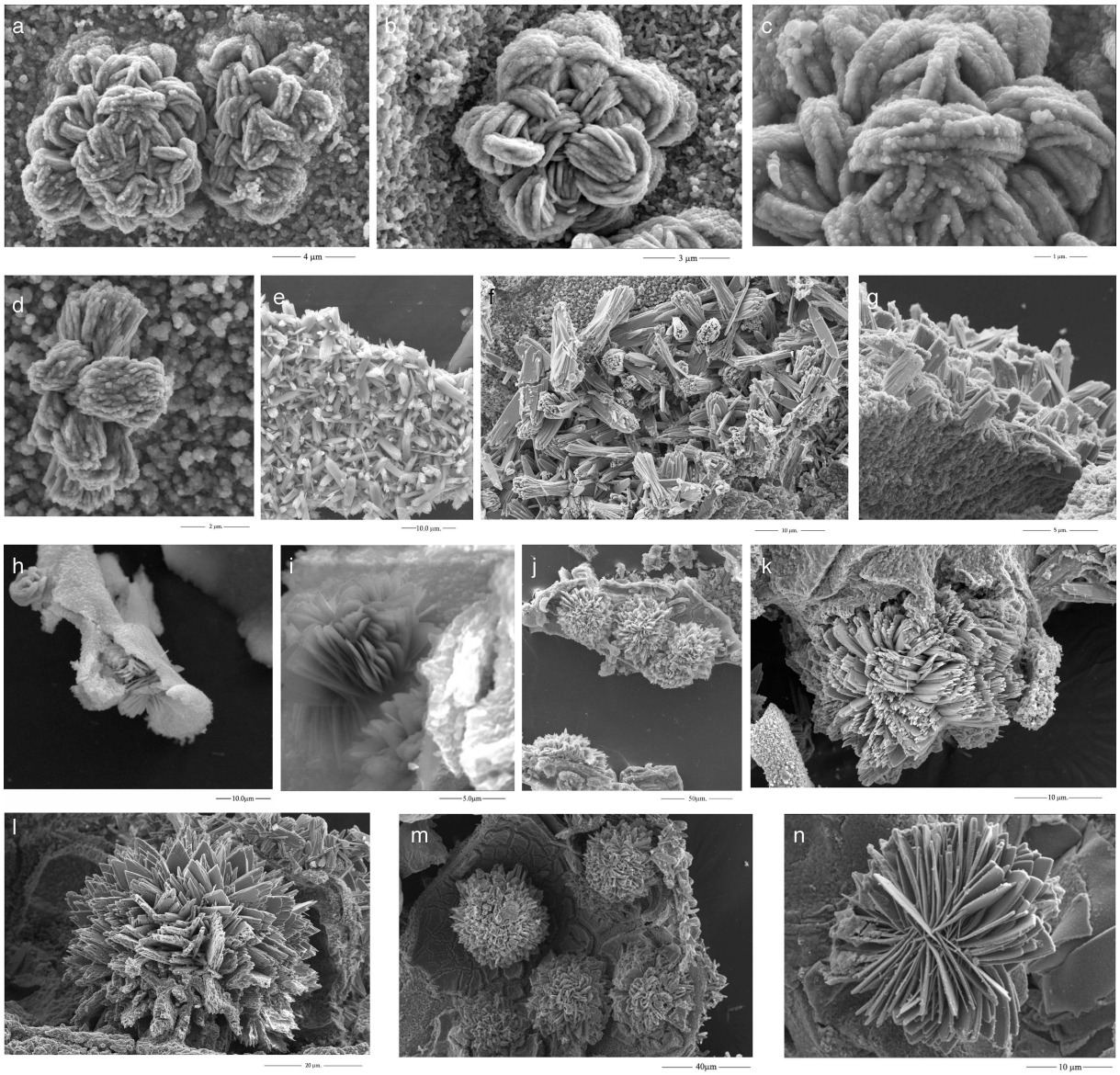

Figure 7. Nanostructures obtained by liquid-liquid phase techniques. ESEM micrographs of structures produced by reverse injection of silicate into $CuSO_4$ solution.

assigned to crystals of $Cu_4(OH)_6SO_4$. These crystals are consistent with the chemical analysis observed above in our microstructures, however our morphology is different to those recently reported.[5] The reflections observed at 28.4°, 30.8°, 35.9°, 36.3°, and 58° (2θ units) can be assigned to crystals of copper oxide, as in the mineral paramelaconite (PDF 03–0879). The reflections at 20.8°, 36.3°, and 42.5° (2θ units) can be assigned to other copper oxide crystals (JCPDS 44–0706). Moreover, reflections found at 16.5°, 23°, 25.5°, 33.5°, 36.3°, and 53° (2θ units) can be assigned to crystals of copper hydroxides; these crystals are metastable and transform easily to copper oxides.[4] However, some of these reflections can be also assigned to the copper sulfate-oxide-hydroxide brochantite, confirming the above Raman results. For a more detailed study, a micro-XRD analysis was performed in a tube formed through the injection technique, where the tube size is large enough to permit this. Some 1 mm diameter spots were analysed in the internal and external surfaces of this tube. The profiles are similar in both surfaces; there existing more amorphous phases in the external surface. Brochantite is the main component with reflections at 16.5°, 22.8°, 27.9°, 30.4°, 33.4°, 34.4°, 35.5°, 36.2°, 37.6°, 39.0°, 39.8°, 41.2°, 42.1°, 43.4°, 46.0°, 50.0°, 52.6°, 59.1°, 60.0°, 61.3°, and 65.1° (2θ units). Some reflections at 8.9°, 9.3°, 10.0°, 12.2°, 18.0°, 21.9°, and 25.0° (2θ units) can be assigned to plancheite, a copper silicate hydrate. In the internal surface, reflections of tenorite, a copper oxide, are observed at 32.3°, 35.5°, 38.8°, 48.8°, and 58.3° (2θ units). Some small reflections can be assigned to the presence of other copper sulfate-hydroxide-hydrates, such as langite and antlerite.

© 2019 Wiley-VCH Verlag GmbH & Co. KGaA, Weinheim

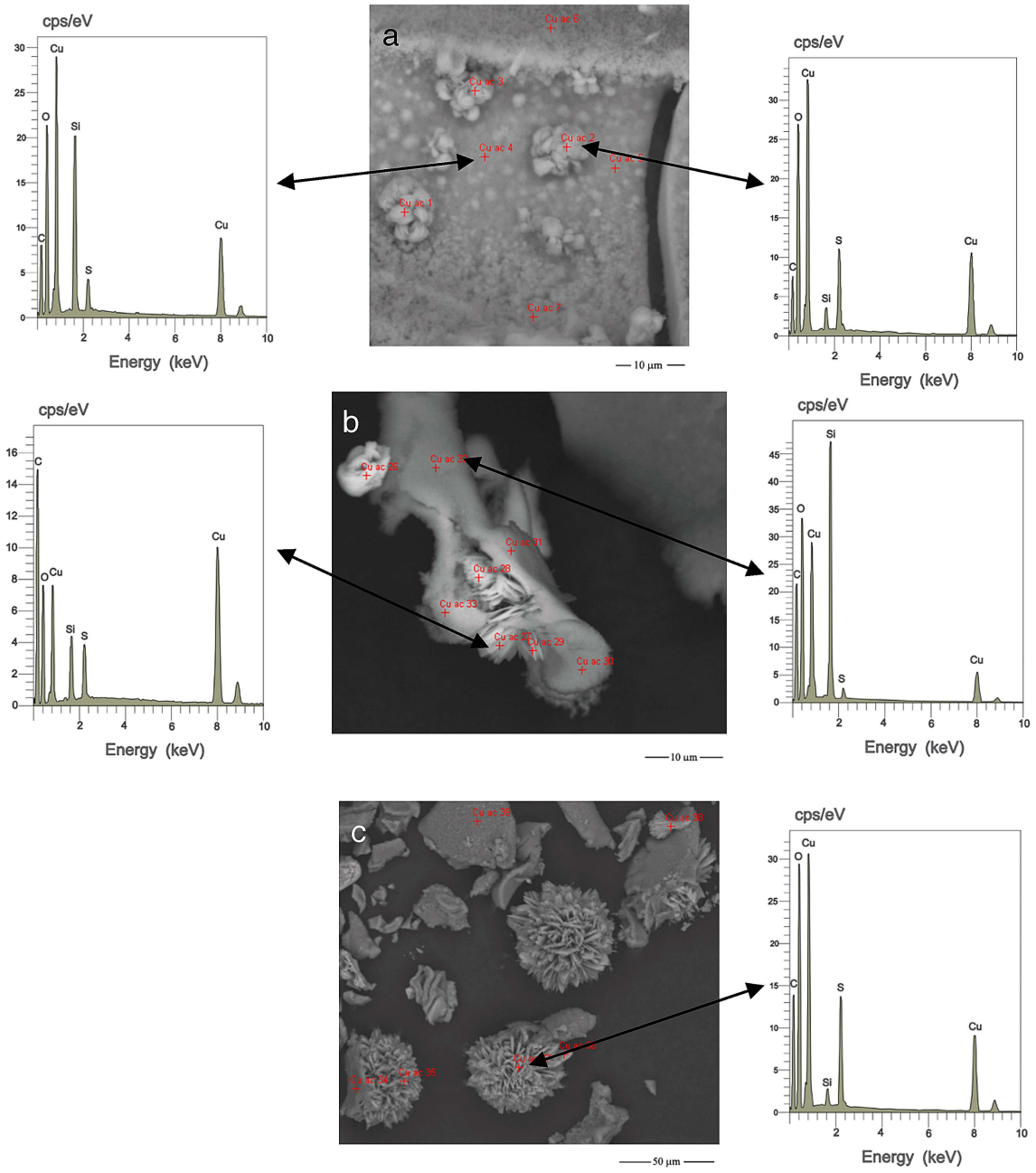

Figure 8. Chemical microanalyses of materials obtained by liquid-liquid phase techniques by reverse injection of silicate into $CuSO_4$ solution.

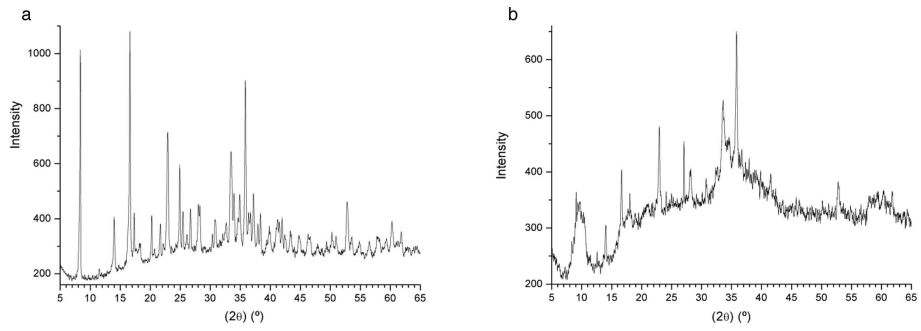

Figure 9. Powder X-ray diffraction analyses of the tubular structures from (a) solid-liquid phase (pellet) and (b) liquid-liquid phase (injection) techniques.

© 2019 Wiley-VCH Verlag GmbH & Co. KGaA, Weinheim

2.4. Discussion

Much research has sought for different morphologies of copper oxides and hydroxides by diverse methods, owing to the important applications of these materials such as catalysis and photodegradation[1–3,13] However, none of these works have reported similar nanostructures to those in the pellet and injection methods described in this work. Recent work[10] has reported hierarchical spheres of copper silicate hydrate from silica spheres and copper salts having different morphology to our nanoflowers. No XRD reflections of the chrysocolla copper silicate hydrate (JCPDS 00–003-1152) can be assigned clearly in our XRD patterns. Previous work has also reported the hierarchical assembly of CuO nanosheets into 3D nanoflowers;[14] however the morphologies were different to those found in this work and the XRD pattern reported, of 32.5°, 36°, 38.5°, 48.5°, 62° (2θ units), does not fit with ours. Our systems are constituted mainly of hydrated copper oxide-hydroxide-sulfates with a low content of sulfate.

A significant research effort is now being applied to investigate the emerging field of chemobrionics, a term that encompasses classical chemical gardens, but is more general, applying to systems that form a self-assembled semipermeable membrane that causes them to continue to self-organize structures through chemical reaction coupled to fluid mechanics and osmosis.[19] The present work constitutes part of the effort to characterize the self-organized material structures that form in chemobrionic systems.[20–24] The advantage of this route to the fabrication of structures is clear: structures self-assembled at room temperature and without using organic additives and hydrothermal conditions. Their morphologies are selectable by changing the preparation conditions.

3. Conclusions

This work reports a method to generate hierarchical nanostructured morphologies of copper oxides and hydroxides at room temperature and without using organic additives and hydrothermal conditions. These morphologies can be selected by changing the preparation conditions. The macroscopic growth of tubular morphologies is different in each method; i.e., from the pellet growth method fine tubes are produced, whereas large, hollow and wide multichannel tubes are formed by the injection method. Nevertheless, in both methods, the microstructure was of a smooth external surface formed principally of silicate and a complex internal surface, in accordance with previous studies.[35] Nanostructure with hierarchical self-assembly at several levels was noted, from nanoparticles to microstructures with varying morphologies. These morphologies are complex and some are biomimetic, resembling flowers, petals, skeins, lentils, and sheaves. A variety of crystal phases are formed in these experiments; these phases are mixed and disordered making complicated their characterization. These morphologies yield greater surface area, providing possible applications in catalysis, photodegradation, support and absorption processes. Hence, these results of the characterization of these morphologies lay the foundations for future works in this direction that should lead to nanotechnological applications.

Experimental Methods

$CuSO_4 \cdot 5H_2O$ and sodium silicate solution at analytical grade were used. Water purified with Mili-Q membranes was used in all cases. The basic solution of sodium silicate was diluted to aliquots of 0.1, 0.5 and 1 M. Aqueous solutions of $CuSO_4$ of 0.5 and 0.25 M were used. The experimental methods may be divided into solid-liquid phase growth and liquid-liquid phase growth.

Solid–Liquid Phases

Two variations were used, having the copper salt seed as an untreated grain or as a fabricated pellet. In the grain method, a raw grain of the hydrated copper salt was introduced into a small reactor with 7 ml of silicate solution. In the pellet method, 200 mg of $CuSO_4 \cdot 5H_2O$ was homogenized with an agate mortar and pressed into cylindrical pellets of 13 mm diameter and 1 mm of thickness using a cell at a pressure of 10 bar over 10 min. The pellet was introduced into a square reactor of 10×30 cm of width and height, respectively. Following which, 45 ml of silicate solution was poured carefully into the reactor. In both methods, after reaction the seed or pellet was left in silicate solution for 20 hours to be sure that all reactants had dissolved completely and all precipitation processes finished. After this time, the silicate was removed and structures were washed twice with water and dried at room temperature (20 °C).

Liquid–Liquid Phases

In this method, two variations were performed: the injection of an aqueous solution of copper sulfate (0.25 or 0.5 M) into a 1 M sodium silicate solution; and the reverse injection of sodium silicate solutions (0.1 or 1 M) into an aqueous solution of copper sulphate (0.25 M). For the injection method two kinds of reactor were used: a tubular reactor of 3 cm diameter and 30 cm in height; and another small square reactor of 5×8 cm in width and height respectively. In both injection experiments a motorized syringe was used. After each growth experiment, the structures formed were washed twice with water to remove the solution and then dried in air at room temperature (20 °C).

Analytical Techniques

After drying, the structures formed were observed with a binocular optical microscope and micrographs of the samples were obtained using Phenom and FEI Quanta 400 environmental scanning electron microscopes (ESEM). Chemical analysis of the micromorphology observed by ESEM was performed in situ in the microscope by using energy-dispersive X-ray spectroscopy (EDX) analysis. Micro-Raman spectroscopy analyses were performed with a JASCO NRS-5100 spectrometer connected to a microscope using a visible/near-infrared (VIS-NIR) laser of 785 nm and 30 mW with 10 cycles of 50 s of acquisition time. Powder X-ray diffraction was performed using a PANalytical X'Pert PRO diffractometer and Cu wavelength. A Bruker D8 Discover microfocus diffractometer with detector PILATUS3R 100 K–A with the Cu K-α wavelength was also used. Identification of the crystallographic phases in diffractograms was performed using the X-Powder program.[36]

© 2019 Wiley-VCH Verlag GmbH & Co. KGaA, Weinheim

Acknowledgements

The authors are grateful to Rafael Esteso for his help and advice. We acknowledge the Spanish MINCINN project grants FIS2016-77692-C2-2P and PCIN-2017-098, along with European FEDER funds and the European COST Action CA17120.

Conflict of Interest

The authors declare no conflict of interest.

Keywords: chemical gardens · chemobrionics · copper hydroxide · copper oxide · nanostructures · self-assembly

[1] Y. Chang, H. C. Zeng, *Cryst. Growth Des.* **2004**, *4*, 397–402.
[2] J. Liu, X. Huang, Y. Li, K. Sulieman, X. He, F. Sun, *J. Mater. Chem.* **2006**, *16*, 4427–4434.
[3] Y. Wang, D. Meng, X. Liu, F. Li, *Cryst. Res. Technol.* **2009**, *44*, 1277–1283.
[4] D. P. Singh, A. K. Ojha, O. N. Srivastava, *J. Phys. Chem. C* **2009**, *113*, 3409–3418.
[5] R. Zhao, T. Yang, M. A. Miller, C. K. Chan, *Nano Lett.* **2013**, *13*, 6055–6063.
[6] N. A. Bakr, T. A. Al-Dhahir, S. B. Mohammad, *J. Adv. Phys.* **2017**, *13*, 4651–4656.
[7] T. Yoshinori, A. Takahisa, *Japan. J. Appl. Phys.* **1990**, *29*, 2388.
[8] A. Pendashteh, M. F. Mousavi, M. S. Rahmanifar, *Electrochim. Acta* **2013**, *88*, 347–357.
[9] Q. Xu, Y. Zhao, J. Z. Xu, J.-J. Zhu, *Sens. Actuators B* **2006**, *114*, 379–386.
[10] X. Wei, C. Tang, X. Wang, L. Zhou, Q. Wei, M. Yan, J. Sheng, P. Hu, B. Wang, L. Mai, *ACS Appl. Mater. Interfaces* **2015**, *7*, 26572–26578.
[11] Z. Huang, F. Cui, H. Kang, J. Chen, X. Zhang, C. Xia, *Chem. Mater.* **2008**, *20*, 5090–5099.
[12] M. B. Gawande, A. Goswami, F.-X. Felpin, T. Asefa, X. Huang, R. Silva, X. Zou, R. Zboril, R. S. Varma, *Chem. Rev.* **2016**, *116*, 3722–3811.
[13] J. Liu, J. Jin, Z. Deng, S.-Z. Huang, Z.-Y. Hu, L. Wang, C. Wang, L.-H. Chen, Y. Li, G. Van Tendeloo, *J. Colloid Interface Sci.* **2012**, *384*, 1–9.
[14] M. Villani, A. B. Alabi, N. Coppede, D. Calestani, L. Lazzarini, A. Zappettini, *Cryst. Res. Technol.* **2014**, *49*, 594–598.
[15] O. Mahapatra, M. Bhagat, C. Gopalakrishnan, K. D. Arunachalam, *J. Exper. Nanosci.* **2008**, *3*, 185–193.
[16] V. V. T. Padil, M. Cerník, *Int. J. Nanomed.* **2013**, *8*, 889–898.
[17] C. A. P. Bastos, N. Faria, A. Ivask, O. M. Bondarenko, A. Kahru, J. Powell, *Nano. Res. Lett.* **2018**, *13*, 111.
[18] K. Korschelt, R. Ragg, C. S. Metzger, M. Kluenker, M. Oster, B. Barton, M. Panthöfer, D. Strand, U. Kolb, M. Mondeshki, *Nanoscale* **2017**, *9*, 3952–3960.
[19] L. M. Barge, S. S. S. Cardoso, J. H. E. Cartwright, G. J. T. Cooper, L. Cronin, A. De Wit, I. J. Doloboff, B. Escribano, R. E. Goldstein, F. Haudin et al., *Chem. Rev.* **2015**, *115*, 8652–8703.
[20] J. H. E. Cartwright, B. Escribano, C. I. Sainz-Díaz, *Langmuir* **2011**, *27*, 3286–3293.
[21] R. Makki, M. Al-Humiari, S. Dutta, O. Steinbock, *Angew. Chem.* **2009**, *121*, 8908–8912; *Angew. Chem. Int. Ed.* **2009**, *48*, 8752–8756.
[22] J. J. Pagano, S. Thouvenel-Romans, O. Steinbock, *Phys. Chem. Chem. Phys.* **2007**, *9*, 110–116.
[23] C. Collins, W. Zhou, J. Klinowski, *Chem. Phys. Lett.* **1999**, *306*, 145–148.
[24] D. Balköse, F. Özkan, U. Köktürk, S. Ulutan, S. Ülkü, G. Nişli, *J. Sol-Gel Sci. Technol.* **2002**, *23*, 253–263.
[25] L. Roszol, R. Makki, O. Steinbock, *Chem. Commun.* **2013**, *49*, 5736–5738.
[26] F. Haudin, V. Brasiliense, J. H. E. Cartwright, F. Brau, A. De Wit, *Phys. Chem. Chem. Phys.* **2015**, *17*, 12804–12811.
[27] E. Rauscher, G. Schuszter, B. Bohner, Á. Tóth, D. Horváth, *Phys. Chem. Chem. Phys.* **2018**, *20*, 5766–5770.
[28] W. Martens, R. L. Frost, J. T. Kloprogge, P. A. Williams, *J. Raman Spectrosc.* **2003**, *34*, 145–151.
[29] I. Almagro, P. Drzymała, K. Berent, C. I. Sainz-Díaz, M. G. Willinger, J. Bonarski, A. G. Checa, *Cryst. Growth Des.* **2016**, *16*, 2083–2093.
[30] P. Ball, *The Self-Made Tapestry: Pattern Formation in Nature*, Cambridge University Press, **2001**.
[31] C. Menor Salván, A. Carmona Ruiz, I. Ramos Márquez, *Acopios: Revista Ibérica de Mineralogía* **2014**, *5*, 1–13.
[32] J. C. Hamilton, J. C. Farmer, R. J. Anderson, *J. Electrochem. Soc.* **1986**, *133*, 739–745.
[33] L. P. Vera Londono, J. A. Pérez Taborda, H. Riascos Landazuri, Análisis espectroscópico *de las películas delgadas de óxido de cobre y del plasma producido por deposición de láser pulsado*, Sociedad Colombiana de Física, **2013**.
[34] F. Haudin, J. H. E. Cartwright, A. De Wit, *J. Phys. Chem. C* **2015**, *119*, 15067–15076.
[35] J. H. E. Cartwright, B. Escribano, S. Khokhlov, C. I. Sainz-Díaz, *Phys. Chem. Chem. Phys.* **2011**, *13*, 1030–1036.
[36] J. D. Martin, *http://www.XPowder.com/index.html*, **2004**.

Manuscript received: April 5, 2019
Version of record online: August 2, 2019

© 2019 Wiley-VCH Verlag GmbH & Co. KGaA, Weinheim